

# Study of the proton-proton collisions at 1683 MeV/c

K. N. Ermakov, V. A. Nikonov, O. V. Rogachevsky, A. V. Sarantsev, V. V. Sarantsev, and S. G. Sherman  
Petersburg Nuclear Physics Institute NRC KI, Gatchina 188300, Russia

Received: date / Revised version: date

**Abstract.** The new data on the elastic  $pp$  and single pion production reaction  $pp \rightarrow pn\pi^+$  taken at the incident proton momentum 1683 MeV/c are presented. The data on the  $pp \rightarrow pn\pi^+$  reaction are compared with predictions from the OPE model. To extract contributions of the leading partial waves the single pion production data are analyzed in the framework of the event-by-event maximum likelihood method together with the data measured earlier.

**PACS.** 13.75.Cs Nucleon-nucleon interactions – 13.85.Lg Total cross sections – 25.40.Ep Inelastic proton scattering

## 1 Introduction

Understanding the proton-proton interaction at low and intermediate energies is the important task of the particle physics. At large momentum transfers where the strong coupling is small, the QCD calculations can be used efficiently for the description of such processes. A large progress was made at low energies where the effective field approach allowed us to describe processes below the resonance region. However the region of the intermediate energies and especially the resonance region is much less accessible for the theoretical calculations and phenomenological dynamic models play the leading role here. The data from the  $NN$  collision reactions forms the basis for the construction of such models which, in turn, have the large range of applications in the nuclear and heavy ion physics.

In the region above the two pion production threshold and up to 1 GeV the  $NN \rightarrow \pi NN$  reaction is dominated by the production of the  $\Delta(1232)$  isobar in the intermediate state. It was natural to suggest that such production is based on the one pion exchange mechanism (OPE) and a set of the corresponding models was put forward [1, 2, 3] a rather long time ago. The pion exchange amplitudes are introduced there using certain form factors with parameters defined from the fit of experimental data. The model of Suslenko et al. describes with a reasonable accuracy (up to normalization factors) the differential spectra of the  $pp \rightarrow pn\pi^+$  and  $pp \rightarrow pp\pi^0$  reactions in the energy region below 1 GeV [2, 4], while the model of Dmitriev et al. was applied to the energies over 1 GeV [3]. In the more complicated model based on the one boson exchange mechanism [5] the dominant contribution for the  $\Delta(1232)$  production is also defined by the one pion exchange: it

was found that other boson exchanges contribute around 10% to the total cross section at the energies above 1 GeV. However it should be noted that there are discrepancies in the simultaneous description of the measured total cross sections for the  $pp \rightarrow pn\pi^+$  and  $pp \rightarrow pp\pi^0$  reactions by the OPE model. For example, at the proton momentum 1683 MeV/c, the OPE model can reproduce well the  $pp \rightarrow pn\pi^+$  measured total cross section with the corresponding choice of the form factor. However, in this case the OPE prediction for the  $pp \rightarrow pp\pi^0$  total cross section will be smaller by about 30% than the experimental one (see Ref. [4]).

Moreover in the region above the incident proton momentum 1.5 GeV/c other contributions start to play a notable role: for example the relatively broad Roper resonance is traced in the spectrum. Therefore for a comprehensive analysis of data it is necessary to apply an approach beyond the OPE model.

With this purpose we perform the partial wave analysis of the data on the single pion production in the framework of the approach based on the work [6]. The result of such an analysis for the lower energy data measured earlier was reported in [8],[9].

In the analysis [9] the several solutions had been found which almost equally described the data. These solutions differ by contributions from the partial waves with high orbital momenta  $L > 3$  which were found to be rather unstable in the fit. It is interesting to compare which solution is compatible with the present higher energy data. It is also interesting to compare the result of the partial wave analysis with the one predicted by the OPE model.

In this paper, we present the new data on the elastic and the  $pp \rightarrow pn\pi^+$  reactions measured at the proton momentum 1683 MeV/c. We compare the data with the OPE model calculations and determine contributions of

Correspondence to: saran@pnpi.spb.ru

the different partial waves from the combined partial wave analysis of the present data and the data measured earlier.

## 2 Experiment

The description of the experiment performed at the PNPI 1 GeV synchrocyclotron was given in details in our previous work [7]. The proton beam was formed by three bending magnets and by eight quadrupole lenses. The mean incident proton momentum value was inspected by the kinematics of the elastic scattering events. The accuracy of the incident momentum value and momentum spread was about 0.5 MeV/c and 7 MeV/c (FWHM) correspondingly with a perfect Gaussian distribution. A total of  $8 \times 10^4$  stereoframes were obtained. The frames were double scanned to search for events due to an interaction of the incident beam. The double scanning efficiency was determined to be 99.95%. Approximately  $7 \times 10^3$  two-prong events were used for the subsequent analysis.

The 2-prong events selected in the fiducial volume of the hydrogen bubble chamber were geometrically reconstructed and kinematically fitted to the following reaction hypotheses:

$$p + p \rightarrow p + p, \quad (1)$$

$$p + p \rightarrow p + n + \pi^+, \quad (2)$$

$$p + p \rightarrow p + p + \pi^0, \quad (3)$$

$$p + p \rightarrow d + \pi^+, \quad (4)$$

$$p + p \rightarrow d + \pi^+ + \pi^0. \quad (5)$$

The events identification procedure was also described in details in [8]. Thus, we list only the most severe criteria here:

1. Events with the confidence level larger than 1% were accepted.
2. Events with only one acceptable hypothesis were identified as belonging to this hypothesis.
3. If several versions revealed a good  $\chi^2$  value, we used the visual estimation of the bubble density of the track to distinguish between proton (deuteron) and pion.

The total number of the 2-prong events which had not passed the reconstruction and fitting procedures was counted to be less than 10%. These unidentified events were apportioned to the fraction of the fitted hypotheses of the accepted events and were used only for the total cross section calculations.

The standard bubble chamber procedure [4] was used to obtain absolute cross sections for the elastic and pion production reactions. The precision in the determination of the millibarn-equivalent was found to be 2%. The cross section values for the inelastic processes together with statistics are listed in Table 1. Let us remind that data on the  $pp \rightarrow pp\pi^0$  reaction at the same energy were published earlier [7].

The differential cross section for the elastic  $pp$  scattering measured in the present experiment is shown in Fig. 1 as open squares with statistical errors. The value of the

**Table 1.** Numbers of events and the total cross sections at the beam momentum 1683 MeV/c. The total elastic cross section was obtained by the interpolation of the differential cross section by the Legendre polynomials. The errors include the statistical errors and millibarn-equivalent ones.

$pp \rightarrow$	events	$\sigma$ mb
elastic	2772	$23.96 \pm 0.57$
$pn\pi^+$	2564	$18.97 \pm 0.57$
$d\pi^+$	57	$0.42 \pm 0.05$
$d\pi^+\pi^0$	7	$0.05 \pm 0.02$

differential cross section for the very forward angle bin is not shown in Fig.1 due a notable loss of events with a slow final proton. If the proton momentum is less than 80 MeV/c the recoil paths is too short to be seen in the bubble chamber. The events with the proton momentum less than 200 MeV/c also might be missing during scanning. Since we do not know the real amendment for these angles we excluded the last forward point and only show the angles where the proton momentum is above 200 MeV/c. In Fig. 1 we compare our elastic differential cross section with the data from the EDDA experiment [10] taken at the incident momentum 1687.5 MeV/c (open red circles). One can see that there is a good agreement between our points and the EDDA data, that supports the correctness of our definition of the millibarn-equivalent.

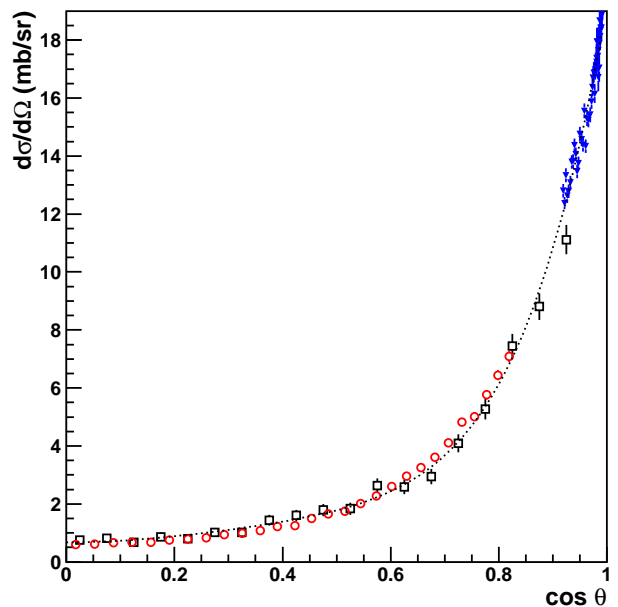


**Fig. 1.** (Color online) Elastic differential cross section. The dotted curve is result of the Legendre polynomial fit of our data (open squares) restricted by the interval  $0 \leq \cos \theta \leq 0.95$  and the data from [11] (blue triangles). The open red circles show the measurements of the EDDA experiment [10] taken at the incident momentum 1687.5 MeV/c.

To obtain the total elastic cross section we applied the following procedure. We fitted the differential cross

section with a sum of even order Legendre polynomials  $A_n P_n(\cos\theta)$   $n = 0, 2, 4, \dots$ . By examining the flatness of the behavior of the fit with decrease of the fitted angular range we determined the range  $0 \leq \cos\theta < 0.95$  as unbiased one. For finding the total elastic cross section we included in the fit above  $\cos\theta = 0.95$  the data from [11] at the incident momentum 1685.7 MeV/c which provide an important constraint for high order polynomials. The result of the fit is shown in Fig. 1 as the dotted curve. The total elastic cross section calculated as  $2\pi A_0$  was found to be  $23.96 \pm 0.57$  mb which is close to the value given in [12].

### 3 The $pp \rightarrow pn\pi^+$ reaction and a comparison with the OPE model

The OPE model [2] describes the single pion production reactions by the four pole diagrams with the  $\pi^0$  or  $\pi^+$  exchanges (we should like to express the deep appreciation to the authors [2] for the accordance of their program code). In this model the intermediate state of the  $\pi N$ -scattering amplitude confines itself to the  $P_{33}$  wave only, assuming the leading role of the  $\Delta_{33}$ -resonance.

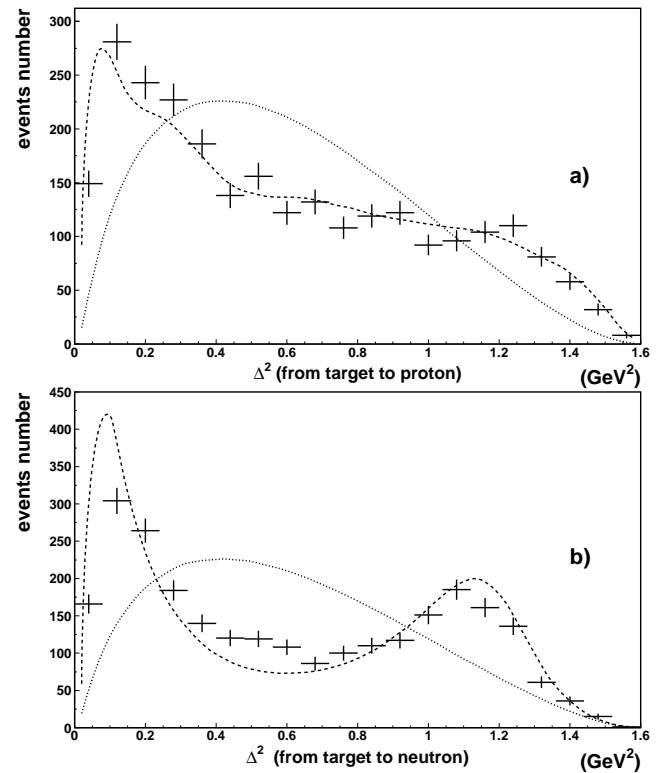
Fig. 2 shows the distributions over the momentum transfer squared,  $\Delta^2 = -(p_t - p_f)^2$ , where  $p_t$  is the four-momentum of the target proton and  $p_f$  is the four-momentum of the final proton or neutron in the  $pp \rightarrow pn\pi^+$  reaction correspondingly. The OPE model calculations normalized to the total number of the experimental events is shown by dashed lines and the shape of the phase volume is shown by dotted lines. One can see that the OPE model describes qualitatively well the  $\Delta^2$  distributions for this reaction.

Fig. 3 presents c.m.s. angular distributions, effective two-particle mass spectra of the final particles and angular distributions in the helicity frame. We would like to point out that the c.m.s. angular distributions are symmetrical ones which is a critical test for the correctness of our event selection.

It is seen that the OPE model calculations normalized to the total number of the experimental events reproduce the particle angular distributions in the c.m.s. of the reaction and the two body mass spectra fairly well. However the angular distributions in the helicity systems show notable deviations from the experimental points.

### 4 Formalism of the partial wave analysis

The partial wave analysis was performed in the framework of the event-by-event maximum likelihood method. The formalism is given in details in [6,13] and based on the spin-orbital momentum decomposition of the initial and final partial wave amplitudes. Therefore it is natural to use the spectroscopic notation  $^{2S+1}L_J$  for two particle partial waves with the intrinsic spin  $S$ , the orbital momentum  $L$  and the total spin  $J$ . Here and below we use  $S, L, J$  for the description of the initial  $NN$  system,  $S_2, L_2, J_2$  for the system of two final particles and  $S', L', J' = J$  for the



**Fig. 2.** Four-momentum transfer  $\Delta^2$  distribution for the  $pp \rightarrow pn\pi^+$  reaction: a) for the transfer to the final proton and b) to neutron. The dashed curves are the OPE calculations and the dotted curves show the shape of the phase volume.

system formed by the two-final particle system and the spectator.

The total amplitude can be written as a sum of partial wave amplitudes as follows [6,13]:

$$A = \sum_{\alpha} A_{tr}^{\alpha}(s) Q_{\mu_1 \dots \mu_J}^{in}(SLJ) A_{2body}^{S_2, L_2, J_2}(s_i) \times Q_{\mu_1 \dots \mu_J}^{fn}(i, S_2 L_2 J_2 S' L' J), \quad (6)$$

where  $Q(S, L, J)$  are operators which describe the system of the initial nucleons,  $A_{tr}^{\alpha}$  is the transition amplitude and  $A_{2body}^{S_2, L_2, J_2}$  describes rescattering processes in the intermediate two-particle channel. The multi-index  $\alpha$  includes all quantum numbers for the description of the definite partial wave,  $s$  is the invariant energy of the initial  $NN$  system squared and  $s_i$  is the invariant energy squared of the two-particle system.

To suppress contributions of amplitudes at high relative momenta we introduced the Blatt-Weisskopf form factors. Thus the energy dependent part of the partial wave amplitudes with production of a resonance, for example, in the two-particle system 12 (e.g.  $\pi p$ ) and the spectator particle 3 ( $n$ ) has the form:

$$A = \frac{A_{tr}^{\alpha} A_{2body}^{S_2, L_2, J_2}(s_{12}) q^L k_3^{L'}}{\sqrt{F(q^2, L, R) F(k_3^2, L', r_3)}}, \quad (7)$$

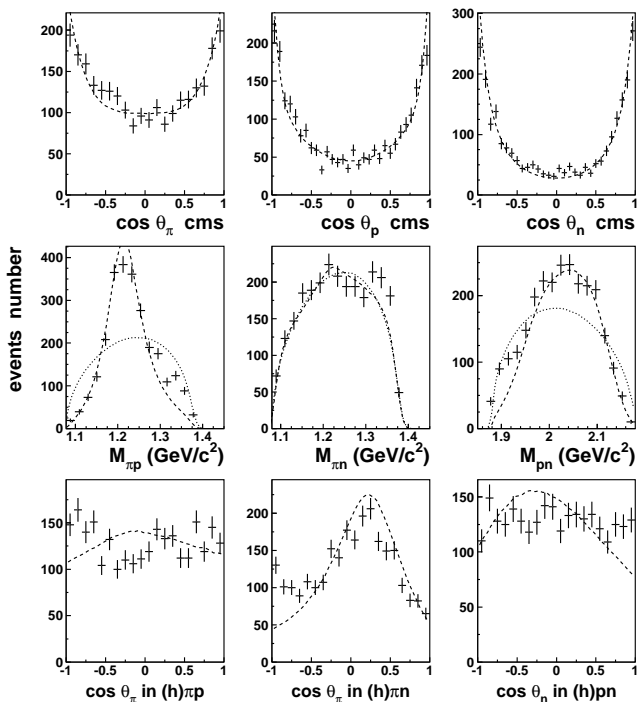


**Fig. 3.** The  $pp \rightarrow pn\pi^+$  data (the crosses with statistical errors): angular distributions of the final particles in the c.m.s. of the reaction (upper line), the effective two-particle mass spectra (middle line) and angular distributions in the helicity systems. The dashed curves show the OPE calculations and dotted curves show the shape of the phase volume.

where  $q$  is the momentum of the incident proton and  $k_3$  is the momentum of the spectator particle, both calculated in c.m.s. of the reaction. The explicit form of the Blatt-Weisskopf form factors  $F(k^2, L, r)$  can be found, for example, in [14]. One should expect that the effective radius of the initial proton-proton system  $R$  should vary between  $1 \div 4$  fm. However, due to a relatively large distance from the  $pp$  threshold it is hard to expect that this value can be determined with a good accuracy in the present analysis. Indeed we did not observe any sensitivity to this parameter and fixed it at 1.2 fm. A very similar result was observed for  $r_3$ . So for our final fits we also fixed this parameter at 1.2 fm.

The combined analysis of the data sets at different energies allows us to extract the energy dependence of the partial waves which is assumed to be a smooth function in this energy interval. This energy dependence was introduced in the following form:

$$A_{tr}^\alpha(s) = \frac{a_1^\alpha + a_3^\alpha \sqrt{s}}{s - a_4^\alpha} e^{ia_2^\alpha}, \quad (8)$$

where  $a_i^\alpha$  are real parameters. The  $a_4^\alpha$  parameters define poles located in the region of left-hand side singularities of the partial wave amplitudes. Such poles are usually a good approximation of the left-hand side cuts defined by the boson exchange diagrams. The phases  $a_2^\alpha$  are defined by contributions from logarithmic singularities connected with three body rescattering in the final state.

For the description of the energy dependence in the  $\pi N$  system we introduce two resonances:  $\Delta(1232)\frac{3}{2}^+$  and Roper  $N(1440)\frac{1}{2}^+$ . The corresponding amplitudes are parameterized as follows:

$$A_{2body}^{S_2, L_2, J_2}(s_{12}) = \frac{k_{12}^{L_2}}{\sqrt{F(k_{12}^2, L_2, r_{12})}} \frac{1}{M_R^2 - s_{12} - M_R \Gamma},$$

$$\Gamma = \Gamma_R \frac{M_R k_{12}^{2L_2+1} F(k_R^2, L_2, r_{12})}{\sqrt{s_{12}} k_R^{2L_2+1} F(k_{12}^2, L_2, r_{12})}. \quad (9)$$

Here  $s_{12}$  is the invariant energy squared in the channel 12,  $k_{12}$  is the relative momentum of the particles 1 and 2 in their rest frame and  $r_{12}$  is the effective radius.

For  $\Delta(1232)$ , we use  $M_R$  and  $\Gamma_R$  taken from PDG [15] with  $r_{12} = 0.8$  fm. The Roper state was parameterized using couplings found in the analysis [16] where the decay couplings of this state into the  $\pi N$ ,  $\Delta\pi$  and  $N(\pi\pi)_{S-wave}$  channels were determined.

For the description of the final  $NN$  interaction we use the following parameterization:

$$A_{2body}^{S_2, L_2, J_2}(s_{23}) = \frac{\sqrt{s_{23}}}{1 - \frac{1}{2} r_{23}^\beta k_{23}^2 a^\beta + i k_{23} a^\beta \frac{k_{23}^{2L_2}}{F(k_{23}^2, r_{23}^\beta, L_2)}}. \quad (10)$$

For the  $S$ -waves it coincides with the scattering-length approximation formula suggested in [17, 18]. Thus the parameter  $a^\beta$  can be considered as the  $NN$ -scattering length and  $r^\beta$  is the effective range of the  $NN$  system.

## 5 Partial wave analysis results and discussion

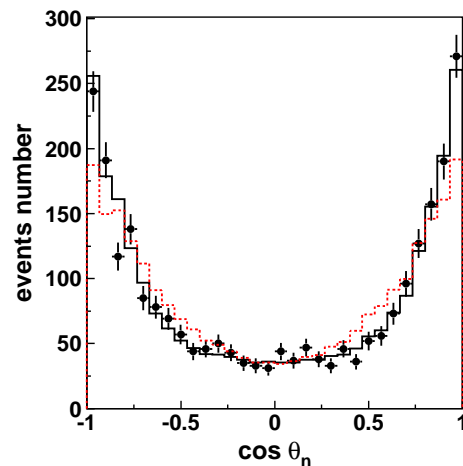


**Fig. 4.** (Color online) The neutron angular distribution calculated in the c.m.s. of the  $pp \rightarrow pn\pi^+$  reaction at 1683 MeV/c. The data are shown by black circles with the statistical errors. The solid (black) histogram shows the prediction from the solution [9] with including partial waves up to  $L = 5$  and the dotted (red) histogram shows the prediction from the solution with  $L$  up to 3.

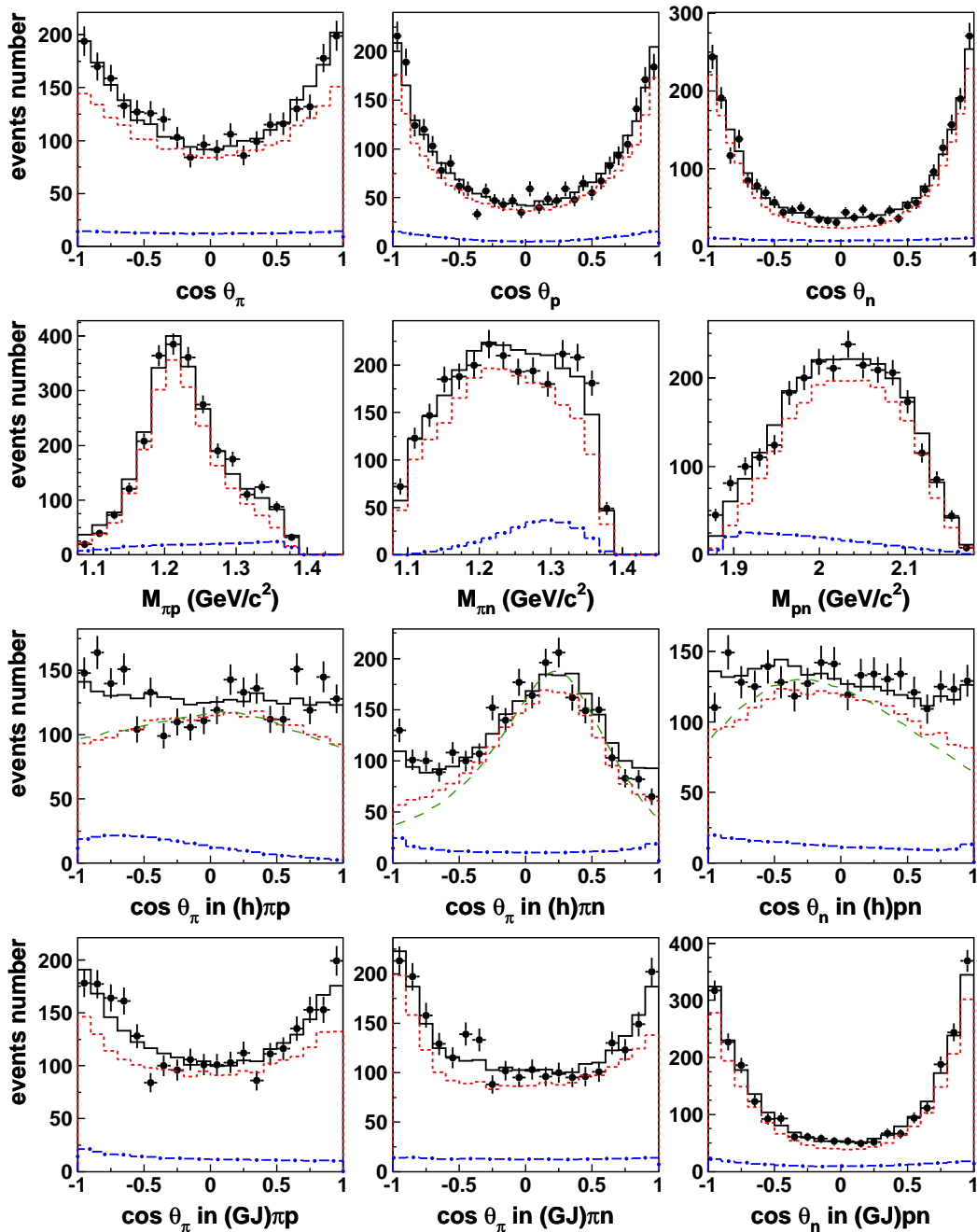


**Fig. 5.** (Color online) The  $pp \rightarrow pn\pi^+$  data taken at the proton momentum 1683 MeV/c with the statistical errors only. First line: the angular distributions of the final particles in the c.m.s. of the reaction. Second line: the effective two-particle mass spectra. Third line: the angular distributions of the final particles in the helicity frame. Fourth line: the angular distributions of the final particles in the Gottfried-Jackson frame. The solid (black) histograms show the result of our partial wave analysis; the dotted (red) and dot-dashed (blue) histograms show the contributions from the production of the  $\Delta(1232)$  and  $N(1440)$  intermediate states. The dashed (green) curves in the helicity frame show the normalized distributions from the OPE model.

We have performed the analysis of the new data starting from our solution obtained in [9]. This solution was restricted by the partial waves with the total spin  $J$  up to 2 and the orbital momentum  $L$  up to 3. This solution produced an acceptable description of the lower energy data but has notable problems in the description of the new data set. For example, the  $\chi^2$  for the normalized angular

distribution of the neutron in the c.m.s. of the reaction is equal to 4.49. The solution fails to describe the extreme angles which are mostly sensitive to partial waves with high orbital momentum. Indeed, the solution with  $L \leq 5$  and  $J \leq 4$  found in [9] (but only used for the error estimation in that paper) predicts the  $\chi^2$  to be 1.23. The description of the data with these two solutions is shown

in Fig. 4. This provides a strong argument for the presence of higher partial waves at studied energy.

Although the solution with  $L \leq 5$  produced a rather good description of the normalized differential cross section, the total cross section predicted by both solutions appeared to be about 10% lower than that given by the data. Therefore we used the last solution as a starting point and performed the combined fit of the present data together with the  $pp \rightarrow pp\pi^0$  data measured earlier [4, 7, 19] and the  $pp \rightarrow pn\pi^+$  data taken at 1628 and 1581 MeV/c [8, 9].

On this way we were able to reproduce both the differential and the total cross sections for all fitted data with a good accuracy. It's worth to note that there is no problem to describe simultaneously the total cross sections for the  $pp \rightarrow pn\pi^+$  and  $pp \rightarrow pp\pi^0$  reactions in this approach.

The result of the partial wave analysis is shown in Fig. 5: the histograms correspond to the Monte Carlo events weighted by the differential cross section calculated from the fit parameters. The  $\chi^2$  for the distributions shown in this picture is varied from 0.65 (for the pion angular distribution in the c.m.s. of the reaction) to 2.6 (for the  $\pi\pi$  invariant mass). We would like to remind that we use the event-by-event maximum likelihood analysis and do not fit directly these distributions.

The partial wave analysis (PWA) reproduces rather well the angular distributions in the helicity system which have systematic deviations in the OPE model. The OPE predictions normalized to the contribution from the  $\Delta(1232)$  production calculated from the PWA solution are shown in Fig. 5 with the dashed lines. It is seen that  $\Delta(1232)$  production from the partial wave analysis and from the OPE model corresponds well each to another. This confirms that  $\Delta(1232)$  is produced by the one pion exchange mechanism and the deviation of the data from the OPE model is due to production of the Roper state.

The present combined analysis found the contributions from the leading initial partial waves to be in a qualitative agreement with the prediction from the solution reported in [9]. However we observe changes for the contributions of the initial partial waves  $^1D_2$  and  $^3F_2$  which are notably increased after the fit of the new data. As concern the partial waves with the total spin  $J = 4$  we found a sizeable contribution from  $^3F_4$ .

For all initial partial waves the contribution of channels with the  $\Delta(1232)$  production varies from 65 to 100% and only for the  $^3P_0$  wave it was found to be rather small one: 12%. The Roper resonance is produced mostly (in the decreasing order of contributions) from the  $^3P_2$ ,  $^3P_0$ ,  $^3P_1$  states and by one order smaller from  $^1S_0$ . We found a notable contribution for the decay of the initial  $^3P_2$  state into the  $(pn)$  subsystem  $^1P_1$  with isospin  $I = 0$ .

To study the stability of the solution we added to the fit partial waves with the total spin  $J$  up to 5 decaying into  $\Delta(1232)N$ . The obtained solution demonstrated some reduction of the contribution from the  $^3P_0$  initial state and increasing the contributions from the  $^3F_2$  state. Taking into account these ambiguities we have performed an error analysis of the initial state contributions to the single pion

production cross sections. For the  $pp \rightarrow pn\pi^+$  reaction these contributions are shown for three incident momenta in Fig. 6.

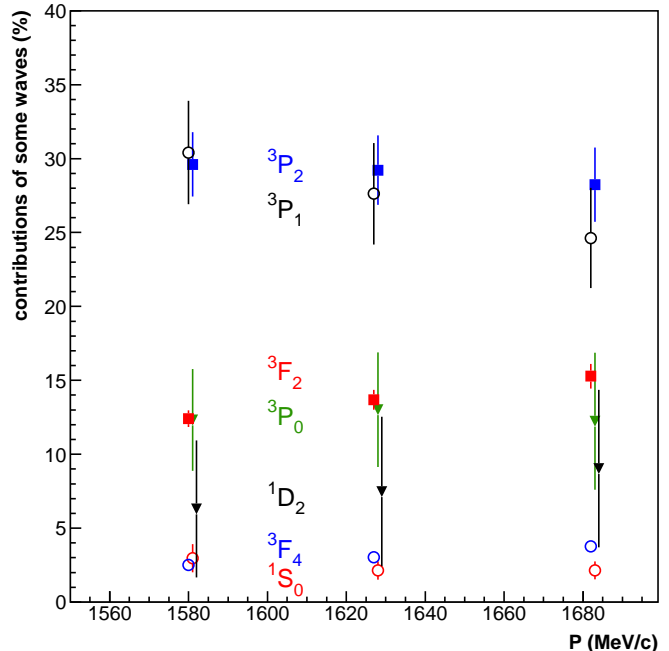


**Fig. 6.** (Color online) Contributions (the percentages) of most important waves in the  $pp \rightarrow pn\pi^+$  reaction.

It is necessary to mention that the present combined analysis defines contributions of the partial waves with smaller errors than it was found in [9]: the unstable contributions from the high spin amplitudes are fixed with the present data.

The obtained solution is well compatible with the data of HADES collaboration on the single pion production at the energy 1.25 GeV [20]: including these data in the combined fit does not change the main results of the analysis and contribution of the partial waves to the HADES data was found to be in the errors given in [20]. The combined analysis of our and HADES data should be a subject of the future joint partial wave analysis.

## 6 Conclusion

The new data on the elastic and  $pp \rightarrow pn\pi^+$  reactions taken at the incident proton momentum 1683 MeV/c are reported. Including these inelastic data in the combined partial wave analysis of the single pion production reactions leads to a better error analysis and therefore to a more precise definition of the partial wave contributions to the  $pp \rightarrow pn\pi^+$  reaction. We observe some changes and in specific transition amplitudes compared to the predictions from the solution [9].

As noted earlier in Ref. [4], although the OPE model provides a qualitative description of most differential distributions, it fails to describe simultaneously the total

cross section of the  $pp \rightarrow pp\pi^0$  and  $pp \rightarrow pn\pi^+$  reactions in the investigated energy region. However our partial wave analysis confirms the dominant role of the  $\Delta(1232)$  production defined by the OPE exchange mechanism. The main source of the discrepancy between OPE and experimental data is due to contribution of other intermediate states, in particular the Roper resonance.

The all analyzed data sets can be downloaded from the Bonn-Gatchina data base [21] as 4-vectors and directly used in the partial wave analysis by other groups. We would like to remind that although we supply a Monte Carlo sample in our web page one can use a standard sample of  $4\pi$  generated events: the bubble chamber events have the efficiency which is close to 100%.

We would like to express our deep gratitude to the bubble chamber staff as well as to laboratory assistants, which toiled at the film scanning and measuring. The work of V.A.Nikonov and A.V.Sarantsev is supported by the RNF grant 16-12-10267.

## References

1. E. Ferrari and F. Selleri, *Nuovo Cimento* **27**, 1450 (1963).
2. V. K. Suslenko and I. I. Gaisak, *Sov. J. Nucl. Phys.* **43**, 252 (1986) [*Yad. Fiz.* **43**, 392 (1986)].
3. V. Dmitriev *et al.*, *Nucl.Phys.* **A459**, 503 (1986).
4. V. P. Andreev *et al.*, *Phys. Rev. C* **50**, 15 (1994).
5. A. Engel *et al.*, *Nucl.Phys.* **A603**, 387 (1996).
6. A. V. Anisovich *et al.*, *Eur. Phys. J. A* **34**, 129 (2007).
7. V. V. Sarantsev *et al.*, *Eur. Phys. J. A* **21**, 303 (2004).
8. K. N. Ermakov *et al.*, *Eur. Phys. J. A* **47**, 159 (2011).
9. K. N. Ermakov *et al.*, *Eur. Phys. J. A* **50**, 98 (2014).
10. D. Albers *et al.*, *Eur. Phys. J. A* **22**, 125 (2004).
11. A. V. Dobrovolsky *et al.*, *Nucl. Phys. B* **214**, 1 (1987).
12. F. Shimizu *et al.*, *Nucl. Phys.* **A386**, 571 (1982).
13. A. V. Anisovich and A. V. Sarantsev, *Eur. Phys. J. A* **30**, 427 (2006).
14. A. Anisovich, E. Klempt, A. Sarantsev and U. Thoma, *Eur. Phys. J. A* **24**, 111 (2005) doi:10.1140/epja/i2004-10125-6 [hep-ph/0407211].
15. J. Beringer *et al.* [Particle Data Group Collaboration], *Phys. Rev. D* **86**, 010001 (2012).
16. A. V. Anisovich *et al.*, *Eur. Phys. J. A* **48**, 15 (2012).
17. K. M. Watson, *Phys. Rev.* **88**, 1163 (1952).
18. A. B. Migdal, *JETP* **1**, 2 (1955).
19. S. A. El-Samad *et al.* [COSY-TOF Collaboration], *Eur. Phys. J. A* **30**, 443 (2006).
20. G. Agakishiev *et al.* [HADES Collaboration], *Eur. Phys. J. A* **51**, no. 10, 137 (2015). doi:10.1140/epja/i2015-15137-5
21. Bonn-Gatchina PWA group: pwa.hiskp.uni-bonn.de

